group-theoretical calculations showing that from a $^2B_{2g}$ ground state transitions would be vibronically allowed only in σ; no π-vibronic spectrum would be had, since there are no a_{1u} or b_{1u} vibrations of the chromophore $TiCl_2O_4$.

In terms of orbital angular-overlap parameters, the proposed energy-level scheme suggests that e_σ' and e_π' for oxygen are greater than the corresponding parameters for chlorine. The order of the σ parameters is that expected from the spectrochemical series. While the ordering of the π values is less evident, it agrees with that found for the analogous Cr(III) complex[2] and that proposed earlier by Barton and Slade.[16]

It may be worth noting that in the spectra of the three complexes, $Cs_2TiCl_5 \cdot 4H_2O$, $Cs_2CrCl_5 \cdot 4H_2O$,[2] and $Cs_3VCl_6 \cdot 4H_2O$,[3] the π spectrum is the stronger in each case. The dichroism is the strongest in the titanium complex and weakest in the chromium complex.

The band that appears as a shoulder 2640 cm^{-1} above the 19 220-cm^{-1} band is most probably due to the coupling of an O–H stretching vibration with the ligand field transition. This vibration notriceably couples only with the upper ligand field state $^2B_{1g}$. In the spectra of some crystals there appears to be one or two other components closer to the band maximum. The distances from the maximum are in the range of other water vibrations. So it may be that more than one water vibration is involved in this shoulder. In the analogous chromium and vanadium complexes a similar band appeared associated also with only one of the ligand field bands, but the symmetry of the bands could not be uniquely determined. The separations in the vanadium and chromium complexes were 2890 and 3070 cm^{-1}, respectively.[2,3]

The difference in maxima in the two polarizations is probably related to the differences in the magnitude of the u vibrations that produce the vibronic bands in the two polarizations.

The ground state ^2E_g will be subject to Jahn–Teller distortion. In D_{4h}' this will become the two Kramers doublets, $E_{1/2g}$ and $E_{3/2g}$; the magnitude and order of this splitting are not known. But the selection rules indicate that transitions to all excited spin–orbit states are vibronically allowed from each ground-state component in both polarizations. So the introduction of spin–orbit coupling will not alter the above arguments.

An attempt was made to fit the observed spectra to the energies calculated for d^1 in D_{4h} symmetry. From the best fit obtained for $Cs_2CrCl_5 \cdot 4H_2O$,[2] we were able to assign the spectra of $Cs_3VCl_6 \cdot 4H_2O$[3] by using the same values of the tetragonal parameters, *Ds* and *Dt*. Calculation of the energies of the present compound using these same values (*Ds* = 239 and *Dt* = 22 cm^{-1}) proved unsuccessful. The tetragonal splitting is calculated to be only 1066 cm^{-1} as compared with the observed value of 4250 cm^{-1}. In the absence of further data, as for example the splitting of the $^2T_{2g}$ (O_h) ground state, no meaningful calculations can be made, since all tetragonal d^1 formulations contain more than two parameters.

Acknowledgment. P.J.M. is grateful to the Research Corp. for a grant for the purchase of the Displex cryogenic refrigerator. M.F.R. thanks the Natural Sciences and Engineering Research Council for operating and equipment grants and is especially grateful to the Atkinson Charitable Foundation and the J. P. Bickell Foundation for grants toward the purchase of the CAD-4 diffractometer.

Registry No. $Cs_2[TiCl_2(H_2O)_4]Cl_3$, 86941-16-4.

Supplementary Material Available: Listings of observed and calculated structure factors and anisotropic thermal parameters and an overall packing diagram (9 pages). Ordering information is given on any current masthead page.

(16) T. J. Barton and R. C. Slade, *J. Chem. Soc., Dalton Trans.*, 650 (1975).

Contribution from the Departments of Chemistry, State University of New York at Buffalo, Buffalo, New York 14214, and University of New Orleans, New Orleans, Louisiana 70148

Electronic Structure of Metalloporphyrins. 2.[1] Experimental Electron Density Distribution of (*meso*-Tetraphenylporphinato)iron(III) Methoxide

CLAUDE LECOMTE,[2a,c] DANA L. CHADWICK,[2a] PHILIP COPPENS,*[2a] and EDWIN D. STEVENS*[2b]

Received November 19, 1982

The crystal structure and experimental electron density distribution of (*meso*-tetraphenylporphinato)iron(III) methoxide, $C_{45}H_{31}N_4OFe$, has been determined from high-resolution single-crystal X-ray diffraction measurements at 100 K. Integrated X-ray intensities were collected with use of Nb-filtered Mo Kα radiation to a resolution of $(\sin\theta)/\lambda = 1.15$ Å^{-1}. Averaging 18 142 symmetry-equivalent reflections from two crystals yielded a set of 8033 independent reflections, which were refined by conventional least-squares to $R = 4.4\%$, $R_w = 5.4\%$. The iron atom is five-coordinate with the oxygen atom of the methoxide ion coordinated in the axial position at a distance of 1.816 (2) Å. The iron is displaced 0.48 Å from the plane of the four nitrogens and 0.56 Å from the mean porphyrin plane. The O–C bond of the methoxide is eclipsed with respect to one of the Fe–N bonds. The experimental electron distribution was determined by least-squares refinement including multipole deformation functions ($R = 2.3\%$, $R_w = 2.8\%$). Populations of the deformation functions in the carbon atoms of the porphyrin ligand agree well with those found previously in (*meso*-tetraphenylporphyrinato)cobalt(II), which suggests transferability of ligand density between complexes. An approximately spherical electron distribution is found at the iron site, and experimental d-orbital occupancies calculated for the iron atom from the deformation populations are consistent with a high-spin Fe(III) state. However, small but significant deviations from spherical symmetry are observed which, together with observed net atomic charges, have been used to calculate a Mössbauer quadrupole splitting constant of +0.6 (3) mm/s.

Introduction

The intense attention that has been devoted to the stereochemistry and electronic structure of metalloporphyrins results from their wide utilization in biological systems. Iron porphyrins have attracted special interest because of their use as a prosthetic group in many proteins, including myoglobin and hemoglobin. For example, in the cooperative binding of dioxygen in hemoglobin, changes both in the electronic structure and in the stereochemistry at the iron site appear to be responsible for the unique biological behavior, and the detailed mechanism is still not fully understood.[3]

(1) Part 1: Stevens, E. D. *J. Am. Chem. Soc.* **1981**, *103*, 5087.
(2) (a) SUNY Buffalo. (b) University of New Orleans. (c) Permanent address: Faculte des Sciences, Laboratoire de Cristallographie, 54506 Vandoeuvreles Nancy, France.

0020-1669/83/1322-2982$01.50/0 © 1983 American Chemical Society

Table I. Experimental Data

$Fe(TPP)OCH_3$ formula	$C_{45}H_{31}N_4OFe$
space group	$P2_1/c$
temp, K	100 (5)
cell dimensions	
a, Å	10.219 (1)
b, Å	15.927 (2)
c, Å	22.345 (3)
β, deg	111.94 (2)
X-ray wavelength, Mo $K\alpha_1$, Å	0.709 30
d(calcd), g/cm^3	1.377 ($Z = 4$)
d(obsd), g/cm^3	1.36 (2)
abs coeff μ, cm^{-1}	4.86
transmission factors, range	0.77–0.84
scan mode	θ:2θ step scans
step size, 2θ, deg	0.04
scan width, deg	2θ($K\alpha_1$) − 1.1 to 2θ($K\alpha_2$) + 1.1
scan speed, s/step	1.0
detector aperture, mm	5 × 5
cryst to detector distance, mm	220
take-off angle, deg	3.0
cryst size, mm	0.25 × 0.47 × 0.45

From structural studies of model compounds and the proteins themselves, many of the stereochemical aspects of the active site in hemoglobin have been examined.[4] In a recent paper,[1] we have demonstrated that accurate experimental information on the electronic structure of metalloporphyrins may also be obtained from careful high-resolution X-ray diffraction measurements. These experiments yield a mapping of the electron distribution, which may be directly analyzed to give information on π-bonding in the ring, metal–ligand covalent bonding, and the distribution of d electrons among the orbitals of the metal atom. The last results are confirmed by independent polarized neutron diffraction measurements, which yield complementary information on the electron spin distribution.[5,6]

In this paper, we report the first high-resolution experimental determination of the electron density distribution in an iron porphyrin, (*meso*-tetraphenylporphinato)iron(III) methoxide, $Fe(TPP)OCH_3$. Future studies will attempt to provide such information on each of the significant oxidation, coordination, and spin states of iron porphyrins.

Experimental Section

Sample Preparation and Data Collection. $Fe(TPP)OCH_3$ was prepared from Fe(TPP)Br and excess piperidine dissolved in CH_2Cl_2 and CH_3OH. After brief boiling, the solution was allowed to cool. Slow evaporation of the solvents yielded relatively large black crystals and long colorless needles. Crystal structure determination identified the black crystals as $Fe(TPP)OCH_3$, apparently produced by the reaction

$$Fe(TPP)Br + CH_3OH + pip \rightarrow Fe(TPP)OCH_3 + pipH^+Br^-$$

A crystal of $Fe(TPP)OCH_3$ was mounted on a Picker FACS-I automatic diffractometer controlled by the Vanderbilt operating system[7] and cooled to 100 ± 5 K with a stream of cold nitrogen gas generated by a locally modified Enraf-Nonius low-temperature device. During measurements, the gas-stream temperature was maintained to within ±1 K at a temperature of 100 ± 5 K as monitored by a copper–constantan thermocouple. Unit cell dimensions were obtained by least-squares refinement on the observed setting angles of the $K\alpha_1$ peaks of 29 centered reflections with $2\theta > 60°$. Scans for systematically absent reflections ($h0l$, $l = 2n + 1$; $0k0$, $k = 2n + 1$) and

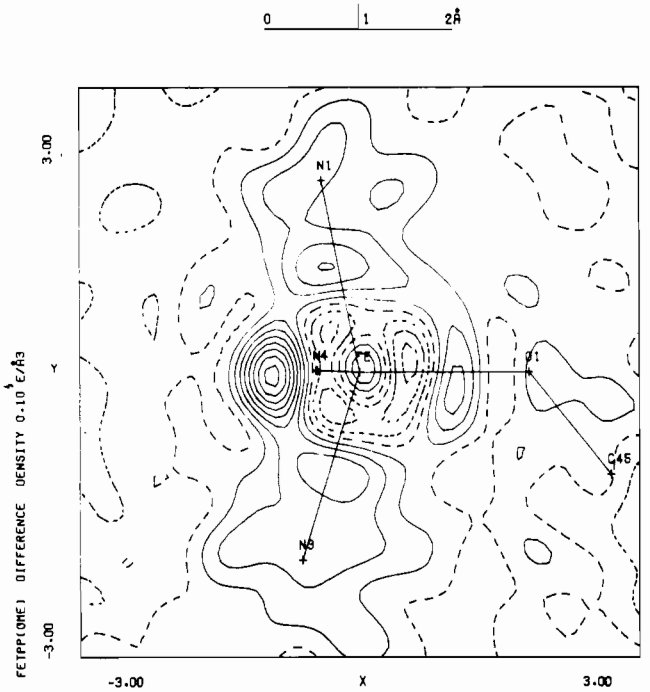

Figure 1. Difference electron density in a plane perpendicular to the porphyrin ring passing through the iron atom and showing a peak corresponding to second fractionally occupied iron site. Contours are plotted at 0.1 e Å^{-3}, intervals, with zero and negative contours shown by dashed lines.

comparison of several symmetry-related reflections uniquely established the space group as $P2_1/c$ with one iron porphyrin molecule in the asymmetric unit. Crystal data for $Fe(TPP)OCH_3$ and experimental conditions are summarized in Table I.

X-ray intensities were obtained with use of a θ:2θ step-scan technique. Each reflection was scanned from 2θ($K\alpha_1$) − 1.1° to 2θ($K\alpha_2$) + 1.1°. The full step-scan profile of each reflection was recorded on magnetic tape and later analyzed to give the integrated intensity and its estimated standard deviation.[8] Eight standard reflections measured after every 100 reflections showed a slow decline in intensity reaching about 10% after the measurement of 9720 reflections, at which time data collection was terminated. Linear least-squares fits to the standard reflection intensities were used to correct the data and to calculate the contribution of scaling to the estimated standard deviations, using a method similar to that of McCandlish, Stout, and Andrews.[9] The data were also corrected for absorption by a numerical Gaussian integration over the crystal volume.[10] Maximum and minimum transmission factors were 0.84 and 0.77, respectively.

Structure Solution and Refinement. The crystal structure was solved by direct methods (MULTAN[11]). After several cycles of full-matrix refinement, difference density maps were calculated revealing the positions of all hydrogen atoms including those of the methoxide ion, thus identifying the axial ligand. All of the hydrogens were included in subsequent refinements with isotropic temperature factors, while anisotropic temperature factors were refined for all other atoms. Core, valence, and total X-ray scattering factors were taken from Hartree–Fock wave functions,[12] except for hydrogen, for which a contracted scattering factor[13] was used. Anomalous scattering factors for Fe, O, N, and C were also included.[14] Each observation was weighted by $w = 1/\sigma^2(F_o)$, where $\sigma(F^2_o)$ was taken to be the larger of $\sigma_{calcd}(F^2)$

(3) Perutz, M. F. *Br. Med. Bull.* **1976**, *32*, 195. Collman, J. P. *Acc. Chem. Res.* **1977**, *10*, 265. Drago, R. S.; Corden, B. B. *Ibid.* **1980**, *13*, 353.
(4) Scheidt, R. W. *Acc. Chem. Res.* **1977**, *10*, 339. Jameson, G. B.; Molinaro, F. S.; Ibers, J. A.; Collman, J. P.; Brauman, J. I.; Rose, E.; Suslick, K. S. *J. Am. Chem. Soc.* **1980**, *102*, 3224.
(5) Williams, G. A.; Figgis, B. N.; Mason, R. *J. Chem. Soc., Dalton Trans.* **1981**, 734.
(6) Coppens, P.; Holaday, A.; Stevens, E. D. *J. Am. Chem. Soc.*, in press.
(7) Lenhert, P. G. *J. Appl. Crystallogr.* **1975**, *8*, 568.
(8) Blessing, R. H.; Coppens, P.; Becker, P. *J. Appl. Crystallogr.* **1974**, *7*, 488.
(9) McCandlish, L. E.; Stout, G. H.; Andrews, L. C. *Acta Crystallogr., Sect. A* **1975**, *A31*, 245.
(10) Coppens, P.; Leiserowitz, L.; Rabinovich, D. *Acta Crystallogr.* **1965**, *18*, 1035.
(11) Germain, G.; Main, P.; Woolfson, M. M. *Acta Crystallogr., Sect. A* **1971**, *A27*, 368.
(12) "International Tables of X-ray Crystallography"; Kynoch Press: Birmingham, England, 1974; Vol. 4.
(13) Stewart, R. F.; Davidson, E. R.; Simpson, W. T. *J. Chem. Phys.* **1965**, *42*, 3175.
(14) Cromer, D. T.; Liberman, D. *J. Chem. Phys.* **1970**, *53*, 1891.

Table II. Data Reduction[a]

$(\sin\theta)/\lambda$ range	$R(F^2)$[b]	$R_w(F^2)$[c]
all reflcns	0.029	0.044
0.00–0.25	0.021	0.034
0.25–0.50	0.024	0.037
0.50–0.80	0.055	0.055
0.80–1.15	0.110	0.110

[a] Total number of reflections 18 142, with 8033 unique reflections. [b] $R(F^2) = \Sigma_i(F_i^2 - \langle F^2\rangle)/\Sigma_i(F_i^2)$. [c] $R_w(F^2) = [\Sigma_i(w_i(F_i^2 - \langle F^2\rangle))^2/\Sigma(w_i F_i^4)]^{1/2}$; $w_i = 1/\sigma^2(F_i^2)$.

$= (\sigma^2_{count} + \sigma^2_{scale} + (0.04F^2_o)^2)^{1/2}$ and $\sigma_{obsd}(F^2) = (\sum_i(\langle F^2\rangle - F_i^2)^2)^{1/2}/N$ for N measurements of symmetry-related reflections. Reflections with both F_{obsd} and F_{calcd} less than 3σ were considered "unobserved" and were not included in the refinement. The conventional refinement converged at $R = 0.039$ and $R_w = 0.049$ for 6159 symmetry-independent reflections ($[(\sin\theta)/\lambda]_{max} = 0.65$ Å^{-1}).

A difference electron density map (Figure 1) calculated by Fourier summation revealed a large residual peak of 1.2 e/Å^3 at fractional coordinates of $x = 0.60$, $y = 0.84$, and $z = 0.64$, below the molecular plane and about 0.95 Å from the iron atom. Since aspherical features of the d-electron density distribution are expected to occur closer to the metal atom (about 0.45 Å in CoTPP[1]), and since the peak is symmetrically located across the porphyrin plane from the iron atom, it has been interpreted as a partial iron atom resulting either from slight disorder in the molecular packing of the type found in Fe(TPP)Cl[15] or possibly from the presence of a small amount of $(FeTPP)_2O$ impurity,[16] although it is difficult to see how it could be accommodated in the lattice.

Peaks associated with an axial ligand on the partial iron atom are not apparent on the difference map, but at least one calculated orientation of a methoxide ion with the carbon atom at $x = 0.650$, $y = 0.936$, $z = 0.553$ results in no intermolecular contacts with either the oxygen or the methyl carbon atom less than 3.5 Å.

Additional data was then collected on a second crystal. In addition to recollection of data with $(\sin\theta)/\lambda < 0.65$ Å^{-1}, high-order reflections in the range $0.65 < (\sin\theta)/\lambda < 1.15$ Å^{-1} were also measured. Since most of the high-order reflections are weak, the results of the previous least-squares refinement were used to predict the intensities of higher order reflections and only those reflections with intensities predicted to be greater than 10 times their estimated standard deviations were measured. Data were collected from all four quadrants, yielding a total of 28 376 reflections. These data were processed in the same manner as the first set. Unfortunately, the number of usable high-order data was limited by the width of their diffraction profiles.

Refinement of the data from the second crystal gave $R = 0.047$ and $R_w = 0.058$ for 7489 reflections ($[(\sin\theta)/\lambda]_{max} = 1.15$ Å^{-1}). A comparison of refined parameters from the two data sets did not show any significant differences. A final difference map calculated from the second data set revealed an almost identical peak at the site of the disordered iron atom. The two data sets were then scaled together with use of their least-squares scale factors and merged (18 142 total reflections) and symmetry-related forms averaged to give a final set of 8033 unique reflections. The internal agreement factors are summarized in Table II. The poor crystal quality and lack of intensity in high-order reflections are responsible for the poor internal agreement at high $(\sin\theta)/\lambda$.

A second iron atom with partial occupancy was then included in a conventional least-squares refinement on the merged data set. The sum of the occupancies of both iron sites was constrained to 1.0. The refinement converged at $R = 0.044$ and $R_w = 0.054$ with a goodness of fit of 1.84. The fractional occupancy of the second iron site was found to be 0.015 (1).

In order to calculate deformation maps of the electron density distribution, it is necessary to obtain positional and thermal parameters for the atoms that are free of bias from the aspherical features of the valence electron distribution.[17] This is frequently achieved by refinements in which only high-order data are included, since the scattering is then primarily due to the core electrons.[18] In this study, such a technique cannot be used because of the insufficient number of high-order reflections. An alternative technique has been applied in which additional parameters are added to the conventional least-squares refinement model which seek to describe the features of the valence electron distribution in terms of a multipole expansion of density functions.[19,20] In the model used here, the electron density at each atom is described by a sum of atom centered deformation functions

$$\rho_{atom}(\mathbf{r}) = \rho_{core}(r) + P_v\rho_{valence}(\kappa r) + \sum_{l=0}^{4} R(\kappa' r)\sum_{m=-l}^{l} P_{lm}y_{lm}(\mathbf{r}/r) \quad (1)$$

where ρ_{core} and $\rho_{valence}$ are spherical Hartree–Fock core and valence densities, the y_{lm} values are spherical harmonic angular functions in real form

$$R_{lm} = Nr^{n(l)}\exp(-\zeta r) \quad (2)$$

where N is a normalization factor and n and ζ are chosen for each l value, as described previously.[20] The P_v, P_{lm}, κ, and κ' values are refinable parameters.

Because of the large number of parameters to be optimized in the multipole model, a number of constraints have been imposed on the population parameters. The populations of chemically equivalent atoms have been constrained to be equal. Other population constraints include C_{4v} symmetry for the iron atom, C_s symmetry for the oxygen atom, C_s symmetry for the nitrogen atoms (mirror plane perpendicular to the pyrrole rings), C_s symmetry for the C_α and C_β carbon atoms (mirror plane in the plane of the pyrrole ring), and C_{2v} symmetry for the C_γ carbon and carbon atoms for the phenyl rings. The multipole expansion was truncated at the octapolar level ($l = 3$) for all carbon atoms, and for hydrogen atoms only a monopole and single dipole directed along the H–C bond were included. Since products of d orbitals correspond to density features with hexadecapolar symmetry ($l = 4$), these parameters were included for the iron and nitrogen atoms.

Three multipole refinements were done, which differ in the model for the electron density near the iron site. The first refinement (refinement I) was an attempt to fit all of the density around the iron site, including the peak on the opposite side of the porphyrin ring, with the density parameters of the iron at a single site. In refinement II, two iron sites were included with occupancies of 0.985 and 0.015. The d-electron distribution on the iron atom was represented by a Hartree–Fock radial function with variable κ and variable total number of d electrons. No density corresponding to 4s electrons was included. The second iron atom was assumed to be spherical.

In refinement III, two iron sites were included as in refinement II, but the d-electron density was represented with a Slater type radial function and the 4s-electron density by a Hartree–Fock radial function. The populations of both the 3d and 4s density functions and the κ of the 3d density function were varied. Because of the large number of parameters, it was necessary to divide the parameters into several large blocks, which were refined in alternate cycles.

Final positional parameters from refinement II are listed in Table III. The corresponding bond distances are tabulated in Table IV and the bond angles in Table V. The multipole parameters from refinements I, II, and III are compared with those of CoTPP in Table VI.

Electron Density Maps. The electron deformation density, defined as the difference between the total observed density and the density corresponding to a superposition of neutral, spherical atoms, $\rho_{obsd}/k - \sum\rho_{spherical\ atoms}$, is sensitive to the redistribution of electrons within the molecule as a result of chemical bonding. The deformation density maps presented here correspond to the density of the least-squares multipole deformation model, rather than the observed density, ρ_{obsd}/k. They are obtained by Fourier summation of structure factors and therefore contain the effects of series termination and smearing by atomic thermal motion. Structure factors missing from the observed X-ray data are included in the dynamic model density to a resolution of $(\sin\theta)/\lambda = 0.85$ Å^{-1}. Since the model deformation density is not calculated directly from the experimental data, noise in the maps due to statistical errors in the X-ray measurements is absent. The degree

(15) Hoard, J. L.; Cohen, G. H.; Glick, M. D. *J. Am. Chem. Soc.* **1967**, *89*, 1992.
(16) Cohen, I. A. *J. Am. Chem. Soc.* **1969**, *91*, 1980.
(17) Coppens, P. *Acta Crystallogr., Sect. B* **1974**, *B30*, 225.
(18) Stewart, R. F.; Jensen, L. H. *Z. Kristallogr., Kristallogeom., Kristallphys., Kristallchem.* **1969**, *128*, 133. Stevens, E. D.; Hope, H. *Acta Crystallogr., Sect. A* **1975**, *A31*, 494.
(19) Dawson, B. *Proc. R. Soc. London, Ser. A* **1967**, *298*, 255. Harel, M.; Hirshfeld, F. L. *Acta Crystallogr., Sect. B* **1975**, *B31*, 162. Stewart, R. F. *Acta Crystallogr., Sect. A* **1976**, *A32*, 565.
(20) Hansen, N. K.; Coppens, P. *Acta Crystallogr., Sect. A* **1978**, *A34*, 909.

Table III. Atomic Fractional Coordinates

atom	*x*	*y*	*z*	atom	*x*	*y*	*z*
Fe	0.530 68 (3)	0.827 98 (1)	0.655 83 (1)	C(37)	0.043 93 (23)	1.164 03 (14)	0.520 49 (11)
O(1)	0.405 12 (13)	0.776 56 (8)	0.683 57 (6)	C(38)	0.130 78 (21)	1.099 26 (13)	0.554 86 (9)
N(1)	0.713 15 (15)	0.821 99 (9)	0.737 05 (6)	C(39)	0.751 13 (19)	1.003 01 (10)	0.852 17 (8)
N(2)	0.611 37 (15)	0.727 39 (9)	0.619 62 (7)	C(40)	0.672 38 (20)	1.019 76 (12)	0.890 17 (9)
N(3)	0.422 55 (15)	0.862 36 (9)	0.560 60 (7)	C(41)	0.733 27 (23)	1.062 62 (12)	0.948 04 (9)
N(4)	0.516 15 (15)	0.954 10 (9)	0.679 13 (7)	C(42)	0.871 83 (21)	1.089 31 (12)	0.968 22 (9)
C(1)	0.749 38 (18)	0.875 39 (11)	0.789 61 (8)	C(43)	0.951 11 (21)	1.073 84 (11)	0.930 89 (9)
C(2)	0.856 80 (10)	0.836 81 (11)	0.844 24 (8)	C(44)	0.890 59 (19)	1.030 83 (19)	0.872 93 (8)
C(3)	0.886 19 (19)	0.761 28 (12)	0.824 81 (8)	C(45)	0.260 79 (24)	0.764 46 (17)	0.651 07 (12)
C(4)	0.797 45 (18)	0.751 69 (11)	0.758 02 (8)	H(2)	0.893 (2)	0.858 (1)	0.885 (1)
C(5)	0.798 09 (18)	0.680 87 (11)	0.720 94 (8)	H(3)	0.949 (3)	0.721 (2)	0.849 (1)
C(6)	0.710 92 (18)	0.670 63 (11)	0.656 10 (8)	H(7)	0.787 (2)	0.553 (1)	0.633 (1)
C(7)	0.719 03 (20)	0.600 97 (12)	0.616 25 (9)	H(8)	0.612 (2)	0.584 (1)	0.518 (1)
C(8)	0.625 33 (20)	0.616 69 (12)	0.555 80 (9)	H(12)	0.269 (2)	0.836 (1)	0.409 (1)
C(9)	0.558 60 (19)	0.695 36 (11)	0.557 74 (8)	H(13)	0.196 (2)	0.968 (1)	0.448 (1)
C(10)	0.458 42 (19)	0.734 83 (11)	0.504 71 (8)	H(17)	0.378 (2)	1.135 (1)	0.662 (1)
C(11)	0.396 17 (19)	0.812 16 (11)	0.506 82 (8)	H(18)	0.557 (3)	1.111 (2)	0.776 (1)
C(12)	0.297 32 (21)	0.853 46 (12)	0.450 90 (8)	H(22)	1.073 (2)	0.682 (1)	0.756 (1)
C(13)	0.263 00 (21)	0.927 26 (12)	0.470 69 (9)	H(23)	1.243 (3)	0.582 (2)	0.804 (1)
C(14)	0.342 42 (18)	0.934 04 (11)	0.538 87 (8)	H(24)	1.176 (3)	0.446 (2)	0.833 (1)
C(15)	0.340 39 (18)	1.004 37 (11)	0.575 91 (8)	H(25)	0.937 (3)	0.422 (2)	0.812 (1)
C(16)	0.423 41 (18)	1.013 66 (11)	0.641 53 (8)	H(26)	0.770 (2)	0.528 (1)	0.760 (1)
C(17)	0.430 64 (20)	1.088 25 (12)	0.678 80 (9)	H(28)	0.603 (3)	0.730 (1)	0.430 (1)
C(18)	0.526 95 (20)	1.074 44 (11)	0.738 76 (9)	H(29)	0.531 (2)	0.687 (1)	0.319 (1)
C(19)	0.580 81 (18)	0.990 54 (11)	0.739 00 (8)	H(30)	0.316 (3)	0.628 (1)	0.267 (1)
C(20)	0.689 82 (18)	0.954 08 (11)	0.790 92 (8)	H(31)	0.157 (3)	0.609 (2)	0.323 (1)
C(21)	0.904 64 (19)	0.614 05 (12)	0.752 73 (8)	H(33)	0.226 (2)	0.656 (1)	0.427 (1)
C(22)	1.047 42 (22)	0.629 07 (14)	0.766 78 (9)	H(34)	0.354 (3)	1.100 (2)	0.482 (1)
C(23)	1.147 29 (23)	0.567 65 (16)	0.796 79 (10)	H(35)	0.200 (3)	1.209 (2)	0.423 (1)
C(24)	1.105 33 (25)	0.491 36 (15)	0.813 06 (10)	H(36)	0.011 (2)	1.249 (1)	0.449 (1)
C(25)	0.964 72 (25)	0.476 10 (14)	0.800 15 (10)	H(37)	−0.030 (3)	1.180 (2)	0.528 (1)
C(26)	0.863 68 (23)	0.537 27 (12)	0.769 75 (9)	H(38)	0.111 (3)	1.068 (1)	0.587 (1)
C(27)	0.420 10 (20)	0.697 15 (11)	0.438 90 (8)	H(40)	0.572 (2)	1.003 (1)	0.874 (1)
C(28)	0.513 36 (22)	0.705 22 (13)	0.406 93 (9)	H(41)	0.680 (2)	1.071 (1)	0.973 (1)
C(29)	0.472 80 (23)	0.679 98 (12)	0.342 86 (9)	H(42)	0.914 (3)	1.121 (2)	1.006 (1)
C(30)	0.341 55 (23)	0.645 27 (12)	0.311 04 (9)	H(43)	1.044 (2)	1.094 (1)	0.944 (1)
C(31)	0.248 07 (23)	0.635 70 (12)	0.342 53 (9)	H(44)	0.941 (2)	1.019 (1)	0.847 (1)
C(32)	0.288 15 (22)	0.662 26 (12)	0.406 32 (8)	H(45)	0.217 (4)	0.822 (2)	0.640 (2)
C(33)	0.247 86 (19)	1.075 78 (11)	0.541 33 (8)	H(46)	0.221 (4)	0.743 (2)	0.677 (2)
C(34)	0.274 73 (20)	1.117 58 (12)	0.491 99 (9)	H(47)	0.247 (4)	0.730 (2)	0.615 (2)
C(35)	0.186 03 (22)	1.181 03 (12)	0.457 27 (10)	Fe(2)	0.597 (2)	0.839 (1)	0.636 (1)
C(36)	0.071 24 (22)	1.204 66 (12)	0.471 79 (10)				

Table IV. Bond Distances and Standard Deviations (Å)

			Iron–Ligand				
$Fe-N_1$	2.0623 (12)	$Fe-N_2$	2.0978 (16)	$Fe-N_3$	2.0726 (14)	$Fe-N_4$	2.0943 (15)
Fe–O	1.8155 (15)	$Fe-Fe_2$	0.96 (2)	Fe_2-N_1	2.14 (2)	Fe_2-N_2	1.84 (2)
Fe_2-N_3	1.98 (2)	Fe_2-N_4	2.36 (2)	$O-C_{45}$	1.393 (2)	$C_{45}-H_{46}$	0.90 (4)
$C_{45}-H_{47}$	0.94 (4)	$C_{45}-H_{45}$	1.00 (3)				
			Porphinato Ring				
C_1-N_1	1.384 (2)	C_6-N_2	1.377 (2)	$C_{11}-N_3$	1.384 (2)	$C_{16}-N_4$	1.382 (2)
C_1-C_2	1.440 (2)	C_6-C_7	1.445 (3)	$C_{11}-C_{12}$	1.440 (2)	$C_{16}-C_{17}$	1.437 (3)
C_2-C_3	1.350 (3)	C_7-C_8	1.356 (2)	$C_{12}-C_{13}$	1.348 (3)	$C_{17}-C_{18}$	1.352 (2)
C_3-C_4	1.437 (2)	C_8-C_9	1.435 (3)	$C_{13}-C_{14}$	1.439 (2)	$C_{18}-C_{19}$	1.444 (3)
C_4-N_1	1.383 (2)	C_9-N_2	1.381 (2)	$C_{14}-N_3$	1.383 (2)	$C_{19}-N_4$	1.380 (2)
C_4-C_5	1.401 (3)	C_9-C_{10}	1.394 (2)	$C_{14}-C_{15}$	1.398 (3)	$C_{19}-C_{20}$	1.400 (2)
C_1-C_{20}	1.398 (2)	C_6-C_5	1.399 (2)	$C_{11}-C_{10}$	1.395 (3)	$C_{16}-C_{15}$	1.401 (2)
C_5-C_{21}	1.498 (2)	$C_{10}-C_{27}$	1.499 (2)	$C_{15}-C_{33}$	1.497 (2)	$C_{20}-C_{39}$	1.495 (2)
C_2-H_2	0.90 (2)	C_7-H_7	1.01 (2)	$C_{12}-H_{12}$	0.92 (2)	$C_{17}-H_{17}$	0.92 (2)
C_3-H_3	0.93 (2)	C_8-H_8	0.96 (2)	$C_{13}-H_{13}$	0.95 (2)	$C_{18}-H_{18}$	0.98 (2)
			Phenyl Groups				
$C_{21}-C_{22}$	1.394 (3)	$C_{27}-C_{32}$	1.387 (3)	$C_{33}-C_{38}$	1.390 (3)	$C_{39}-C_{40}$	1.397 (3)
$C_{22}-C_{23}$	1.392 (3)	$C_{27}-C_{28}$	1.395 (3)	$C_{34}-C_{33}$	1.401 (3)	$C_{40}-C_{41}$	1.388 (3)
$C_{23}-C_{24}$	1.382 (4)	$C_{28}-C_{29}$	1.393 (3)	$C_{34}-C_{35}$	1.386 (3)	$C_{41}-C_{42}$	1.383 (3)
$C_{24}-C_{25}$	1.377 (4)	$C_{29}-C_{30}$	1.378 (3)	$C_{35}-C_{36}$	1.381 (3)	$C_{42}-C_{43}$	1.385 (3)
$C_{25}-C_{26}$	1.397 (3)	$C_{30}-C_{31}$	1.391 (4)	$C_{36}-C_{37}$	1.382 (4)	$C_{43}-C_{44}$	1.390 (2)
$C_{26}-C_{21}$	1.391 (3)	$C_{31}-C_{32}$	1.395 (3)	$C_{37}-C_{38}$	1.390 (3)	$C_{44}-C_{39}$	1.396 (3)
$C_{22}-H_{22}$	0.94 (2)	$C_{28}-H_{28}$	0.96 (2)	$C_{34}-H_{34}$	0.97 (3)	$C_{40}-H_{40}$	0.99 (2)
$C_{23}-H_{23}$	0.96 (3)	$C_{29}-H_{29}$	0.93 (3)	$C_{35}-H_{35}$	0.93 (3)	$C_{41}-H_{41}$	0.92 (3)
$C_{24}-H_{24}$	1.00 (2)	$C_{30}-H_{30}$	0.96 (3)	$C_{36}-H_{36}$	0.94 (2)	$C_{42}-H_{42}$	0.94 (2)
$C_{25}-H_{25}$	0.97 (3)	$C_{31}-H_{31}$	0.97 (2)	$C_{37}-H_{37}$	0.88 (4)	$C_{43}-H_{43}$	0.94 (2)
$C_{26}-H_{26}$	0.91 (2)	$C_{32}-H_{32}$	0.92 (3)	$C_{38}-H_{38}$	0.95 (3)	$C_{44}-H_{44}$	0.93 (3)

Table V. Bond Angles and Standard Deviations (deg)

				Iron-Ligand			
N_1-Fe-N_2	87.02 (6)	N_1-Fe-N_4	87.14 (5)	N_2-Fe-N_3	86.62 (6)	N_3-Fe-N_4	86.67 (6)
N_1-Fe-N_3	151.20 (6)	N_2-Fe-N_4	154.57 (7)	O_1-Fe-N_1	101.56 (6)	O_1-Fe-N_2	102.67 (6)
O_1-Fe-N_3	107.24 (6)	O_1-Fe-N_4	102.88 (7)	Fe-O_1-C_{45}	129.10 (9)	O_1-C_{45}-H_{45}	107 (2)
O_1-C_{45}-H_{46}	111 (2)	O_1-C_{45}-H_{47}	109 (2)	H_{46}-C_{45}-H_{45}	102 (3)	H_{46}-C_{45}-H_{47}	112 (3)
				Macrocycle			
C_1-N_1-C_4	105.9 (1)	C_6-N_2-C_9	106.0 (1)	C_{11}-N_3-C_{14}	105.9 (1)	C_{16}-N_4-C_{19}	105.8 (1)
N_1-C_1-C_2	109.6 (1)	C_5-C_6-C_7	124.6 (2)	N_3-C_{11}-C_{12}	109.6 (2)	C_{15}-C_{16}-C_{17}	125.1 (2)
C_1-C_2-C_3	107.3 (1)	N_2-C_6-C_5	125.5 (2)	C_{11}-C_{12}-C_{13}	107.3 (2)	N_4-C_{16}-C_{17}	109.9 (1)
C_2-C_3-C_4	107.4 (1)	N_2-C_6-C_7	109.8 (1)	C_{12}-C_{13}-C_{14}	107.5 (2)	N_4-C_{16}-C_{15}	125.0 (2)
C_3-C_4-N_1	109.7 (1)	C_6-C_7-C_8	106.9 (2)	C_{13}-C_{14}-N_3	109.6 (2)	C_{16}-C_{17}-C_{18}	107.5 (2)
C_3-C_4-C_5	124.0 (1)	C_7-C_8-C_9	107.3 (2)	C_{13}-C_{14}-C_{15}	124.1 (2)	C_{17}-C_{18}-C_{19}	106.8 (2)
N_1-C_4-C_5	126.2 (1)	C_8-C_9-C_{10}	125.1 (2)	N_3-C_{14}-C_{15}	126.2 (1)	C_{18}-C_{19}-C_{20}	124.8 (2)
N_1-C_1-C_{20}	126.0 (1)	N_2-C_9-C_{10}	125.0 (2)	N_3-C_{11}-C_{10}	126.6 (1)	N_4-C_{19}-C_{20}	125.0 (2)
C_{20}-C_1-C_2	124.4 (2)	N_2-C_9-C_8	109.9 (1)	C_{10}-C_{11}-C_{12}	123.7 (2)	N_4-C_{19}-C_{18}	110.0 (1)
C_4-C_5-C_{21}	117.0 (1)	C_9-C_{10}-C_{11}	124.7 (2)	C_{14}-C_{15}-C_{33}	116.7 (1)	C_{19}-C_{20}-C_1	124.9 (2)
C_6-C_5-C_{21}	118.5 (2)	C_9-C_{10}-C_{27}	119.6 (2)	C_{16}-C_{15}-C_{33}	118.6 (2)	C_{19}-C_{20}-C_{39}	118.3 (2)
C_4-C_5-C_6	124.4 (2)	C_{11}-C_{10}-C_{27}	115.6 (1)	C_{14}-C_{15}-C_{16}	124.6 (2)	C_1-C_{20}-C_{39}	116.7 (1)
				Phenyl Groups			
C_{22}-C_{21}-C_{26}	119.1 (2)	C_{32}-C_{27}-C_{28}	119.0 (2)	C_{34}-C_{33}-C_{15}	119.7 (2)	C_{44}-C_{39}-C_{40}	119.1 (2)
C_{26}-C_{21}-C_5	121.0 (2)	C_{32}-C_{27}-C_{10}	121.5 (2)	C_{34}-C_{33}-C_{38}	118.8 (2)	C_{44}-C_{39}-C_{20}	119.8 (2)
C_{22}-C_{21}-C_5	119.9 (2)	C_{28}-C_{27}-C_{10}	119.2 (2)	C_{38}-C_{33}-C_{15}	121.4 (2)	C_{40}-C_{39}-C_{20}	121.1 (2)
C_{21}-C_{22}-C_{23}	120.4 (2)	C_{27}-C_{28}-C_{29}	120.2 (2)	C_{33}-C_{34}-C_{35}	120.5 (2)	C_{39}-C_{40}-C_{41}	120.1 (2)
C_{22}-C_{23}-C_{24}	120.1 (2)	C_{28}-C_{29}-C_{30}	120.3 (2)	C_{34}-C_{35}-C_{36}	120.2 (2)	C_{40}-C_{41}-C_4	120.2 (2)
C_{23}-C_{24}-C_{25}	120.1 (2)	C_{29}-C_{30}-C_{31}	120.2 (2)	C_{35}-C_{36}-C_{37}	119.8 (2)	C_{41}-C_{42}-C_{43}	120.5 (2)
C_{24}-C_{25}-C_{26}	120.2 (2)	C_{30}-C_{31}-C_{32}	119.3 (2)	C_{36}-C_{37}-C_{38}	120.5 (2)	C_{42}-C_{43}-C_{44}	119.5 (2)
C_{21}-C_{26}-C_{25}	120.2 (2)	C_{27}-C_{32}-C_{31}	121.0 (2)	C_{37}-C_{38}-C_{33}	120.2 (2)	C_{43}-C_{44}-C_{39}	120.7 (2)

to which the model density agrees with the experimental density can be judged by inspection of the residual density, defined by

$$\rho_{\text{residual}} = \rho_{\text{obsd}}/k - \rho_{\text{model}}$$

For a sufficiently flexible model, the residual density should show only random noise. The significance of features in the residual density can be judged by comparison with a plot of the distribution of the estimated standard deviation in the deformation density, which includes contributions from the uncertainty in the X-ray intensities, the scale factor, and the refined parameters.[21,22] Except near nuclear positions, the estimated standard deviation is approximately 0.05 e/Å^3.

Results and Discussion

Description of the Molecular Structure. An ORTEP[23] plot of Fe(TPP)OCH_3 at 100 K, in which the numbering scheme is defined, is shown in Figure 2. As with other five-coordinate iron(III) porphyrins, the coordination of the iron atom is square pyramidal, with the oxygen atom of the methoxide ion in the axial position 1.8155 (15) Å from the iron. This is slightly shorter than the Fe–O bond length of 1.842 (4) Å found by Hoard et al.[24] in the structure of the dimethyl ester of (mesoporphyrin IX)iron(III) methoxide, Fe(Meso)OCH_3, and lies intermediate between the Fe–O distances (1.75 (2) and 1.898 (7) Å) reported for two dioxygen complexes of iron(II) "picket fence" porphyrins.[4b] The Fe–O–C angle of 129.10 (9)° is also somewhat different from the corresponding angle in Fe(Meso)OCH_3 (125.9 (6)°) but remarkably close to the Fe–O–O angles (131 (2) and 129 (2)°) in the two dioxygen complexes.[4b]

The iron atom in Fe(TPP)OCH_3 lies 0.562 (1) Å above the least-squares plane of the porphyrin ring and 0.484 (1) Å above the plane of the four nitrogen atoms. The corresponding distances in Fe(Meso)OCH_3 were reported to be 0.490 and 0.455 Å.[24] Least-squares planes are given in Table VII (supplementary material). These displacements indicate a small but significant doming of the porphyrin toward the metal atom and are similar to those found in other five-coordinate high-spin iron(III) porphyrins.[25]

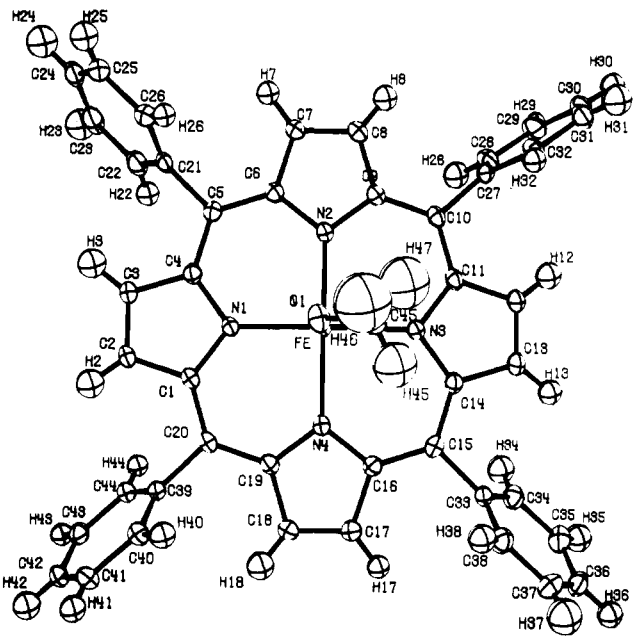

Figure 2. ORTEP plot of the Fe(TPP)OCH_3 molecule viewed down the axial direction. Thermal ellipsoids are plotted at the 50% probability level. The numbering scheme for all atoms in the asymmetric unit is shown.

An interesting feature of the molecular structure is the eclipsed configuration of the methoxide ion with respect to the Fe–N(3) bond. This is in contrast to the perfectly staggered configuration adopted by the methoxide ion in Fe(Meso)-OCH_3. Small axial ligands such as O_2 and NO also adopt staggered configurations in iron porphyrins, while larger ligands such as pyridine and imidazole often assume an intermediate configuration, probably as a compromise between steric and electronic factors.[4] The lack of consistency in the orientations observed for the methoxide ion suggests that neither steric nor electronic factors are sufficiently strong to dictate the orientation, and the observed geometry may simply

(21) Rees, B. *Acta Crystallogr., Sect. A* **1976**, *A32*, 483.
(22) Stevens, E. D.; Coppens, P. *Acta Crystallogr., Sect. A* **1976**, *A32*, 915.
(23) Johnson, C. K. *Oak Ridge Natl. Lab.* [*Rep.*] *ORNL (U.S.)* **1965**, *ORNL-5138*.
(24) Hoard, J. L.; Hamor, M. H.; Hamor, T. A.; Caughey, W. D. *J. Am. Chem. Soc.* **1965**, *87*, 2312.
(25) Hoard, J. L. In "Porphyrins and Metalloporphyrins"; Smith, K. M., Ed.; Elsevier: Amsterdam, 1975; pp 317–380.

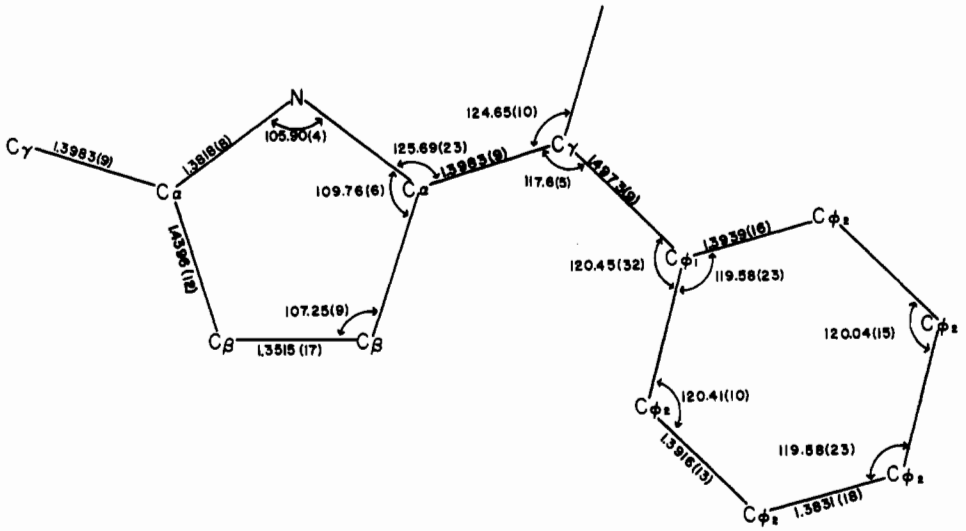

Figure 3. Average bond distances (in angstroms) and angles (in degrees) in the tetraphenylporphyrin ring of Fe(TPP)OCH_3. The atom labels identify the chemically unique atoms for which valence deformation functions have been determined.

reflect the relatively weak crystal-packing forces.

The oxygen atom is slightly displaced from the ideal axial position toward N(1), resulting in unequal N(1)–Fe–O(1) and N(3)–Fe–O(1) angles (101.56 (6) and 107.24 (6)°, respectively) and an angle between the normal to the porphyrin plane and the Fe–O bond of 2.9 (1)°, while the N(2)–Fe–O(1) and N(4)–Fe–O(1) angles are essentially equal. A similar effect is evident in the Fe–N bond lengths. The Fe–N(2) and Fe–N(4) distances (2.0978 (16) and 2.0943 (15) Å) are nearly equal and longer than the Fe–N(1) and Fe–N(3) distances (2.0632 (12) and 2.0726 (14) Å). The molecule thus possesses an approximate mirror plane containing the methoxide ion. The agreement between equivalent bond distances and angles in the rest of the porphyrin molecule is excellent. Average values are given in Figure 3. The close agreement between chemically equivalent distances and angles is an indication of the validity of the refinement model. All bond distances are within 2 standard deviations of the average value. The largest variation is found in the C_α–C_γ–$C_{\phi 1}$ angle.

Multipole Refinements. Each of the multipole refinements results in a significantly better fit to the data than the conventional spherical-atom least-squares model. The large magnitudes of the P_{10}, P_{20}, P_{30}, and P_{40} population parameters on iron in refinement I reflect the attempt of the model to fit the density at the second iron site. While it is fairly successful at doing so, the result is a density that corresponds to an unrealistically diffuse d orbital (ζ = 2.63 bohr^{-1} compared with an optimized value of 3.73 bohr^{-1} calculated for a neutral isolated high-spin iron atom[26]).

Refinements II and III, in which partial occupancy of the second iron site is included, yield more realistic ζ values and much smaller multipole populations for iron, indicating little distortion from a spherical density distribution as expected for a high-spin iron atom. Small populations have also been found for the high-spin iron atom in $KFeS_2$,[27] while much larger populations are found for low-spin iron, such as in FeS_2.[28] Residual maps calculated after refinement III (Figures 4 and 7) show only random noise at a level that agrees well with the estimated error in the deformation density.

All three refinements yield very similar population parameters for the atoms of the macrocycle. Furthermore, they agree

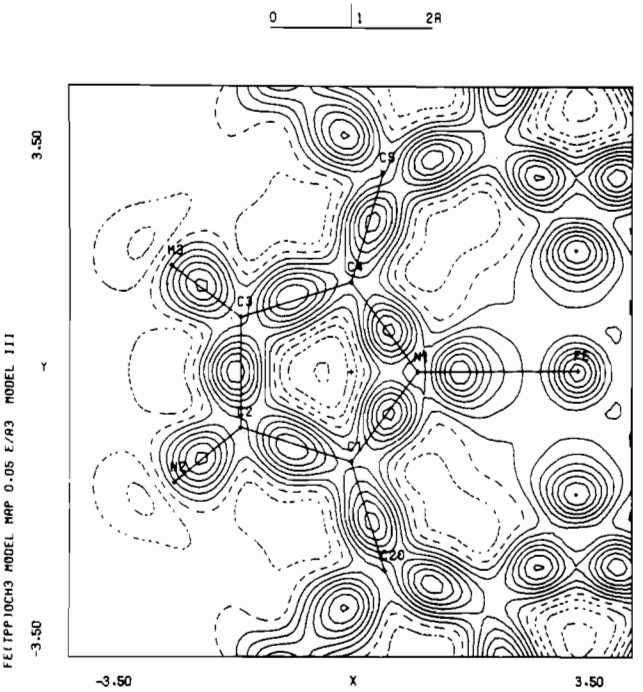

Figure 4. Contour map of the dynamic model deformation density of Fe(TPP)OCH_3 calculated in the plane of one of the pyrrole rings. Contours are plotted at 0.05 e Å^{-3} intervals, with zero and negative contours shown by dashed lines.

remarkably well with the results from CoTPP[1] for all atoms in the porphyrin ring except nitrogen, where the square-pyramidal coordination of Fe(TPP)OCH_3 differs significantly from the square-planar coordination of CoTPP. This suggests that the population parameters and the corresponding deformation density will prove to be transferable among other metalloporphyrins. A similar transferability of the deformation densities of molecular fragments has been demonstrated among smaller molecules by Hirshfeld.[29]

The monopole populations from a deformation refinement formally yield the distribution of atomic charges. Since the net atomic charge on an atom in a molecule is a defined rather than a real physical property, the values obtained depend on the method by which the density is partitioned. Since the deformation parameters are often not localized, we have found

(26) Clementi, E.; Raimondi, D. L. *J. Chem. Phys.* **1963**, *38*, 2686.
(27) Stevens, E. D., to be submitted for publication. Stevens, E. D. "Electron Distributions and the Chemical Bond"; Coppens, P., Hall, M., Eds.; Plenum Press: New York, 1982.
(28) Stevens, E. D.; DeLucia, M. L.; Coppens, P. *Inorg. Chem.* **1980**, *19*, 813.
(29) Hirshfeld, F. L. *Isr. J. Chem.* **1977**, *16*, 198.

Table VI. Multipole Populations

	Fe(TPP)OCH_3 refinement				Fe(TPP)OCH_3 refinement		
	I	II	III		I	II	III
% R	2.31	2.26	2.27	% R_wF^2	5.68	5.59	5.58
% R_w	2.84	2.81	2.79	GOF	1.04	1.02	1.02
% R	4.38	4.22	4.26	scale factor	0.8162 (5)	0.8154 (5)	0.8152 (5)

	Fe(TPP)OCH_3 refinement			CoTPP[1] (low spin)		Fe(TPP)OCH_3 refinement			CoTPP[1] (low spin)
	I	II	III			I	II	III	
				Iron (C_{4v}) (CoTPP D_{4h})					
n_l[a]	4, 4, 4, 4, 4	4, 4, 4, 4, 4	4, 4, 4, 4, 4	4, 4, 4, 4, 4	P_{10}	−0.25 (2)	−0.14 (1)	−0.16 (2)	0.00
κ	1.000	0.810 (5)	1.000	1.000	P_{20}	0.27 (2)	−0.06 (2)	−0.04 (2)	0.80 (4)
$\zeta\kappa'$, bohr^{-1}	5.27 (5)	5.69 (4)	6.50 (4)	7.61 (3)	P_{30}	−0.16 (2)	−0.06 (2)	−0.07 (2)	0.00
P_{val}	0.79 (16)	5.48 (4)	0.47 (15)	0.00	P_{40}	0.26 (3)	0.08 (3)	0.08 (3)	−0.40 (4)
P_{00}	5.23 (4)		5.00 (4)	7.00	P_{44+}	0.01 (2)	0.02 (3)	0.01 (3)	−0.26 (4)
				Nitrogen (C_s) (CoTPP C_{2h})					
n_l	2, 2, 2, 3, 4	2, 2, 2, 3, 4	2, 2, 2, 3, 4	2, 2, 2, 3, 4	P_{31+}	−0.24 (1)	−0.20 (1)	−0.24 (1)	0.03
κ	0.954 (4)	0.954 (3)	0.955 (4)	0.97 (1)	P_{31-}	−0.02 (1)	−0.01 (1)	−0.01 (1)	0.00
$\zeta\kappa'$, bohr^{-1}	3.31 (8)	3.70 (8)	3.47 (8)	2.16 (7)	P_{33+}	0.02 (1)	0.01 (1)	0.02 (1)	0.40 (6)
P_{val}	5.84 (2)	5.87 (2)	5.85 (2)	5.77 (9)	P_{33-}	−0.05 (1)	−0.05 (1)	−0.06 (1)	0.00
P_{11+}	0.00 (1)	0.01 (1)	0.00 (2)	0.16 (7)	P_{40}	−0.04 (1)	−0.04 (2)	−0.05 (2)	0.15 (4)
P_{11-}	0.01 (1)	0.01 (1)	0.01 (1)	0.00	P_{42+}	0.07 (1)	0.07 (2)	0.08 (2)	0.06 (4)
P_{20}	0.01 (2)	0.01 (2)	0.01 (2)	−0.42 (5)	P_{42-}	0.04 (1)	0.04 (1)	0.04 (1)	0.00
P_{22+}	0.16 (2)	0.16 (2)	0.16 (2)	0.20 (5)	P_{44+}	0.03 (1)	0.01 (1)	0.02 (1)	0.26 (5)
P_{22-}	0.07 (2)	0.07 (2)	0.07 (1)	0.00	P_{44-}	0.01 (1)	0.00 (1)	0.01 (1)	0.00
				C_α (C_s)					
n_l	2, 2, 2, 3	2, 2, 2, 3	2, 2, 2, 3	2, 2, 2, 3	P_{22+}	−0.02 (1)	−0.01 (1)	−0.02 (1)	−0.01 (2)
κ	1.052 (5)	1.053 (5)	1.059 (5)	1.03 (1)	P_{22-}	−0.01 (1)	−0.01 (1)	−0.01 (1)	0.10 (2)
$\zeta\kappa'$, bohr^{-1}	3.42 (14)	3.26 (15)	3.63 (14)	3.82 (16)	P_{31+}	−0.01 (1)	−0.01 (1)	−0.01 (1)	0.00 (2)
P_{val}	3.53 (2)	3.56 (2)	3.52 (2)	3.98 (13)	P_{31-}	−0.02 (1)	−0.02 (1)	−0.02 (1)	−0.02 (2)
P_{11+}	−0.04 (1)	−0.03 (1)	−0.04 (1)	−0.05 (2)	P_{33+}	0.15 (1)	0.15 (1)	0.13 (1)	0.20 (2)
P_{11-}	−0.01 (1)	−0.01 (1)	−0.02 (1)	0.05 (2)	P_{33-}	0.04 (1)	0.04 (1)	0.04 (1)	0.01 (2)
P_{20}	−0.05 (1)	−0.05 (1)	−0.04 (1)	−0.14 (2)					
				C_β (C_s)					
n_l	2, 2, 2, 3	2, 2, 2, 3	2, 2, 2, 3	2, 2, 2, 3	P_{22+}	0.00 (1)	0.00 (1)	−0.00 (1)	−0.01 (2)
κ	0.990 (4)	0.991 (4)	1.023 (4)	1.01 (1)	P_{22-}	0.05 (1)	0.05 (1)	0.05 (1)	−0.08 (2)
$\zeta\kappa'$, bohr^{-1}	2.93 (6)	2.85 (7)	3.03 (5)	2.95 (10)	P_{31+}	−0.01 (1)	−0.00 (1)	−0.01 (1)	−0.04 (3)
P_{val}	4.34 (2)	4.34 (2)	4.34 (2)	4.26 (11)	P_{31-}	0.03 (1)	0.03 (1)	0.02 (1)	−0.02 (3)
P_{11+}	0.06 (1)	0.06 (1)	0.05 (1)	0.03 (3)	P_{33+}	0.32 (1)	0.34 (1)	0.30 (1)	0.24 (3)
P_{11-}	−0.02 (1)	−0.01 (1)	−0.02 (1)	0.10 (3)	P_{33-}	0.08 (1)	0.08 (1)	0.08 (1)	0.12 (3)
P_{20}	−0.18 (1)	−0.19 (1)	−0.16 (1)	−0.19 (2)					
				C_γ (C_{2v})					
n_l	2, 2, 2, 3	2, 2, 2, 3	2, 2, 2, 3	2, 2, 2, 3	P_{20}	−0.15 (1)	−0.16 (1)	−0.14 (1)	0.14 (2)
κ	0.986 (5)	0.987 (4)	1.001 (5)	1.04 (1)	P_{22+}	0.01 (1)	0.01 (1)	0.01 (1)	−0.06 (2)
$\zeta\kappa'$, bohr^{-1}	3.24 (12)	3.13 (12)	3.44 (11)	4.34 (36)	P_{31+}	−0.03 (1)	−0.02 (1)	−0.03 (1)	−0.03 (2)
P_{val}	4.51 (3)	4.52 (3)	4.50 (3)	4.00 (15)	P_{33+}	0.28 (1)	0.30 (1)	0.26 (1)	0.13 (3)
P_{11+}	−0.07 (1)	−0.07 (1)	−0.06 (1)	−0.06 (2)					
				C_{ϕ_1} (C_{2v})					
n_l	2, 2, 2, 3	2, 2, 2, 3	2, 2, 2, 3	2, 2, 2, 3	P_{20}	−0.12 (1)	−0.13 (1)	−0.11 (1)	−0.31 (4)
κ	1.017 (5)	1.016 (4)	1.023 (5)	0.98 (1)	P_{22+}	0.04 (1)	0.04 (1)	0.03 (1)	−0.01 (3)
$\zeta\kappa'$, bohr^{-1}	2.71 (10)	2.63 (10)	2.83 (9)	2.53 (9)	P_{31+}	−0.04 (1)	−0.04 (1)	−0.04 (1)	−0.04 (5)
P_{val}	3.97 (4)	4.00 (4)	3.98 (4)	4.52 (11)	P_{33+}	0.24 (1)	0.24 (1)	0.22 (1)	0.48 (4)
P_{11+}	−0.03 (1)	−0.05 (1)	−0.03 (1)	−0.09 (4)					
				C_{ϕ_2} (C_{2v})					
n_l	2, 2, 2, 3	2, 2, 2, 3	2, 2, 2, 3	2, 2, 2, 3	P_{20}	−0.16 (1)	−0.17 (1)	−0.15 (1)	−0.25 (2)
κ	0.996 (4)	0.997 (4)	1.001 (3)	1.00 (1)	P_{22+}	0.05 (1)	0.05 (1)	0.03 (1)	0.02 (2)
$\zeta\kappa'$, bohr^{-1}	2.79 (4)	2.71 (4)	2.88 (4)	2.62 (5)	P_{31+}	0.03 (1)	0.04 (1)	0.04 (1)	0.03 (2)
P_{val}	4.22 (3)	4.20 (3)	4.18 (3)	3.91 (6)	P_{33+}	−0.27 (2)	−0.27 (1)	−0.25 (1)	−0.38 (2)
P_{11+}	−0.05 (1)	−0.05 (1)	−0.04 (1)	0.02 (2)					
				O (C_s)					
n_l	2, 2, 2, 3	2, 2, 2, 3	2, 2, 2, 3		P_{22+}	0.03 (2)	0.04 (3)	0.09 (2)	
κ	0.940 (5)	0.933 (5)	0.940 (5)		P_{22-}	0.06 (2)	0.07 (3)	0.06 (2)	
$\zeta\kappa'$, bohr^{-1}	2.85 (11)	2.93 (11)	2.81 (10)		P_{31+}	0.12 (3)	0.10 (3)	0.09 (3)	
P_{val}	6.36 (4)	6.50 (4)	6.41 (4)		P_{31-}	−0.02 (3)	−0.02 (3)	−0.03 (3)	
P_{11+}	0.21 (2)	0.22 (2)	0.24 (2)		P_{33+}	0.05 (3)	0.08 (3)	0.10 (3)	
P_{11-}	−0.03 (2)	0.02 (2)	−0.03 (2)		P_{33-}	−0.05 (3)	−0.03 (3)	−0.03 (3)	
P_{20}	0.04 (3)	0.02 (3)	0.00 (2)						
				C_{45} (1)					
n_l	2, 2, 2, 3	2, 2, 2, 3	2, 2, 2, 3		P_{11+}	0.00 (3)	0.00 (3)	−0.03 (3)	
κ	0.95 (6)	0.925 (5)	0.903 (4)		P_{20}	−0.10 (3)	−0.13 (3)	−0.11 (3)	
$\zeta\kappa'$, bohr^{-1}	2.85 (9)	2.49 (11)	2.55 (11)		P_{30}	0.54 (5)	0.55 (5)	0.54 (5)	
P_{val}	4.24 (7)	3.77 (7)	4.15 (6)		P_{33+}	0.07 (4)	0.07 (4)	0.08 (4)	

Table VI (*Continued*)

	$Fe(TPP)OCH_3$ refinement			$CoTPP^1$ (low spin)		$Fe(TPP)OCH_3$ refinement			$CoTPP^1$ (low spin)
	I	II	III			I	II	III	
				H_β ($C_{\infty v}$)					
n_l	0, 1	0, 1	0, 1	0, 1	P_{val}	0.75 (5)	0.74 (5)	0.76 (5)	1.10 (10)
κ	1.12 (3)	1.12 (3)	1.12 (3)	1.04 (5)	P_{10}	0.13 (2)	0.15 (2)	0.11 (2)	0.30 (3)
$\zeta\kappa'$, $bohr^{-1}$	2.00 (14)	1.91 (14)	2.08 (13)	2.33 (21)					
				$H_{\phi 2}$ ($C_{\infty v}$)					
n_l	0, 1	0, 1	0, 1	0, 1	P_{val}	0.78 (4)	0.76 (4)	0.82 (4)	0.79 (6)
κ	1.14 (3)	1.15 (3)	1.12 (2)	1.14 (5)	P_{10}	0.11 (2)	0.12 (2)	0.11 (2)	0.27 (3)
$\zeta\kappa'$, $bohr^{-1}$	2.08 (8)	2.04 (8)	2.06 (8)	1.91 (18)					
				H (methoxy) ($C_{\infty v}$)					
n_l	0, 1	0, 1	0, 1		P_{val}	0.93 (6)	1.06 (6)	1.01 (6)	
κ	1.05 (5)	1.00 (5)	1.00 (5)		P_{10}	0.32 (3)	0.38 (3)	0.31 (3)	
$\zeta\kappa'$, $bohr^{-1}$	2.00 (14)	1.93 (14)	2.08 (13)						

[a] As defined in eq 2.

that monopole-only refinements frequently yield more consistent net atomic charges than full multipole refinements.[30] Nevertheless, atomic charges from the multipole refinements, especially refinement III, yield quite reasonable values. The experimental populations of the iron 3d and 4s shells are 5.00 (4) and 0.47 (15), respectively, yielding a net charge on the iron atom of 2.5 (2)+ in reasonable agreement with the formal oxidation state. The valence monopole populations for the oxygen, carbon, and hydrogen atoms of the methoxide ligand yield a total net charge of 0.6 (2)−, again in general agreement with the formal charge of 1−. The remaining negative charge is located primarily on the pyrrole nitrogen atoms, which have net charges of 0.85 (2)−. Within the porphyrin molecule, net atomic charges alternate and generally decrease in magnitude with distance from the center of the molecule.

d-Orbital Occupancies. Apparent occupancies of the d orbitals of transition-metal atoms may be derived from the population parameters of the metal atom obtained in a multipole refinement of the X-ray data. This analysis is dependent on several assumptions: a minimal set of d orbitals is an adequate basis for the d electrons, and overlap terms due to covalent interactions between the metal and ligand atoms may be neglected. Within the limits of these approximations, the apparent d-orbital orbital occupancies, P_1, P_2, P_3, and P_4 in electrons, such that $\rho_{3d} = P_1(d_{x^2-y^2})^2 + P_2(d_{z^2})^2 + P_3(d_{xy})^2 + {}^1/_2P_4(d^2_{xz} + d^2_{yz})$, are related to the multipole populations P_{lm} by the following set of linear equations:[31]

$$P_{00} = (1/4\pi)^{1/2}C_{00}(P_1 + P_2 + P_3 + P_4)$$

$$P_{20} = (5/196\pi)^{1/2}C_{20}(-2P_1 + 2P_2 - 2P_3 + P_4)$$

$$P_{40} = (1/196\pi)^{1/2}C_{40}(P_1 + 6P_2 + P_3 - 4P_4)$$

$$P_{44+} = (5/28\pi)^{1/2}C_{44}(-P_1 + P_3)$$

where $C_{lm} = N_{lm}(\text{wave function})/N_{lm}(\text{density function})$. The ratios of the normalization factors N_{lm} enter in these expressions since the density functions are not normalized in the same manner as the wave functions. Note that C_{4v} symmetry has been assumed for the iron atom and that the expressions remain the same as in the case of CoTPP, for which D_{4d} symmetry was assumed. Solving these four equations yields the d-orbital occupancies as a function of the multipole population parameters.

In Table VIII the orbital populations resulting from each of the multipole refinements are given. The effects of correlation between the least-squares parameters are included in the estimated standard deviations. In each case the orbital occupancies are close to those expected for a high-spin electron configuration.

In CoTPP, occupancy of crystal-field-destabilized orbitals has been attributed primarily to covalent interaction between metal and ligand orbitals.[6] Metalloporphyrins and other transition-metal complexes have also been shown to have many low-lying excited states,[32] and a mixing of other spin-state configurations may also result in noninteger occupation numbers. In the case of $Fe(TPP)OCH_3$, the effects of covalent bonding between the metal and ligand atoms on the observed d-orbital occupancies are less obvious, in part due to the angle between the $d_{x^2-y^2}$ orbital and the porphyrin nitrogen atoms. A small covalent contribution to the observed occupancies, however, is reasonable and consistent with the experiment.

Electric Field Gradient. One of the most widely used probes of the electronic structure of iron porphyrins has been Mössbauer spectroscopy. Information on electronic structure is expressed in the Mössbauer experiment primarily in the quadrupole splitting, which results from the interaction of the nuclear quadrupole moment with the electric field gradient at the iron nucleus, and in the isomer shift, which is sensitive to changes in the s-electron density at the iron nucleus. The electron density at an atomic nucleus is not well determined in an X-ray diffraction experiment. However, the electric field gradient at a nucleus arises from the aspherical distribution of electrons in the valence orbitals and the surrounding net atomic charges in the molecule and crystal lattice. Since both d-orbital occupancies and net atomic charges have been determined from the X-ray diffraction data on $Fe(TPP)OCH_3$, a comparison with the Mössbauer quadrupole splitting is possible.

The quadrupole splitting of the Mössbauer spectra is given by

$$\Delta E_{QS} = {}^1/_2e^2qQ(1 + \eta^2/3)^{1/2}$$

where $eq = V_{zz}$ is the principal component of the electric field gradient tensor, Q is the nuclear quadrupole moment, and η is the asymmetry parameter. The electric field gradient is usually divided into lattice and valence contributions

$$q = (1 - \gamma_\infty)q_{lat} + (1 - R)q_{val}$$

where γ_∞ and R are Sternheimer antishielding factors.

Mössbauer studies of a large number of high-spin ($S = {}^5/_2$) iron(III) porphyrins show quadrupole splittings of ~0.6 mm/s with a relatively small spread.[33,34] Also the sign V_{zz} has been

(30) Coppens, P.; Guru Row, T. N.; Leung, P.; Stevens, E. D.; Becker, P. J.; Yang, Y. W. *Acta Crystallogr., Sect. A* **1974**, *A35*, 63.

(31) Stevens, E. D. In "Electron and Magnetization Densities in Molecules and Crystals"; Becker, P., Ed.; Plenum Press: New York, 1980; p 823. Holladay, A.; Leung, P.; Coppens, P. *Acta Crystallogr., Sect. A* **1983**, *A39*, 377–387.

(32) Lin, W. C. In "The Porphyrins"; Dolphin, D., Ed.; Academic Press: New York, 1979; Vol. IV, pp 355–377.

Table VIII. $Fe(TPP)OCH_3$ d-Orbital Occupancies

	atomic orbital	obsd from refinement II	obsd from refinement III	expected (high spin)
P_1	b_1 ($d_{x^2-y^2}$)	1.15 (6)	1.04 (6)	1.00
P_2	a_1 (d_{z^2})	1.15 (5)	1.07 (6)	1.00
P_3	b_2 (d_{xy})	1.21 (6)	1.08 (6)	1.00
P_4	e (d_{xz}, d_{yz})	1.98 (6)	1.81 (8)	2.00

determined to be positive in several five-coordinate high-spin complexes, including Fe(TPP)OMe. The origin of the observed magnitude of the quadrupole splitting and the sign of V_{zz} has been the subject of some discussion,[34] which can now be clarified by analysis of the experimental electron density distribution.

Since a pure high-spin iron atom would have equal d-orbital populations resulting in $q_{val} = 0$, it has generally been assumed that q_{lat} alone is responsible for the observed quadrupole splitting. Crystal field calculations of q_{lat} do predict a positive V_{zz}, with larger contributions from charges in the porphyrin plane than from the axial ligand.[35] However, the observed quadrupole splitting appears to require an unrealistically large crystal field distortion. Simple molecular orbital calculations, on the other hand, incorrectly predict both sign and magnitude of q_{val}.[36]

From the X-ray multipole analysis both q_{val} and q_{lat} may be calculated directly. Since C_{4v} symmetry at the iron site has been assumed, $\eta = 0$ and $V_{xx} - V_{yy} = 0$, and the electric field gradient may be calculated from the quadrupole population, P_{20}, by using[27]

$$eq_{val} = V_{zz,val} = -\tfrac{6}{5}(3^{1/2}P_{20})\zeta^3 e/[n_l(n_l + 1)(n_l + 2)]$$

Taking $P_{20} = -0.044$ (21) and $\zeta = 6.50$ (4) $bohr^{-1}$ from refinement III yields $eq_{val} = +7.6$ (35) $\times 10^{14}$ esu cm^{-3}. The "lattice" contribution due to atomic charges within the molecule is given by the summation

$$eq_{lat} = -e\sum_i P_{00,i}^{net}(3\cos^2\theta_i - 1)/r_i^3$$

where $P_{00,i}^{net}$ is the net atomic charge, r_i the distance from the iron nucleus, and θ_i the angle between r_i and the axial direction. The monopole populations from refinement III yield $eq_{lat} = +0.35$ (15) $\times 10^{14}$ esu cm^{-3}. Charges from atoms in other molecules in the crystal make a negligible contribution. A quantitative comparison of the quadrupole splitting predicted from these X-ray results is hampered by the uncertainty in the values of γ_∞, R, and Q. However, taking reasonable values ($\gamma_\infty = -10$, $R = 0.22$, and $Q = 0.2 \times 10^{-24}$ cm^2) gives $\Delta E_{QS} \approx +0.6$ mm/s compared with the measured value for Fe(TPP)OCH_3 of $|\Delta E_{QS}| = 0.56 \pm 0.05$ mm/s.[37]

Thus, the experimental electron density distribution of $Fe(TPP)OCH_3$ deduced from the X-ray data indicates the observed magnitude of the quadrupole splitting may be attributed to a combination of a valence contribution and a slightly smaller lattice contribution, both with $V_{zz} > 0$. The valence contribution arises from a slight aspherical d-electron distribution, probably due to covalent interactions between the metal atom and ligand atoms, although mixing with other spin states is also a possible explanation. Contributions to eq_{lat} from the axial ligand are opposite to those from charges in the porphyrin plane, with the in-plane contributions dominant.

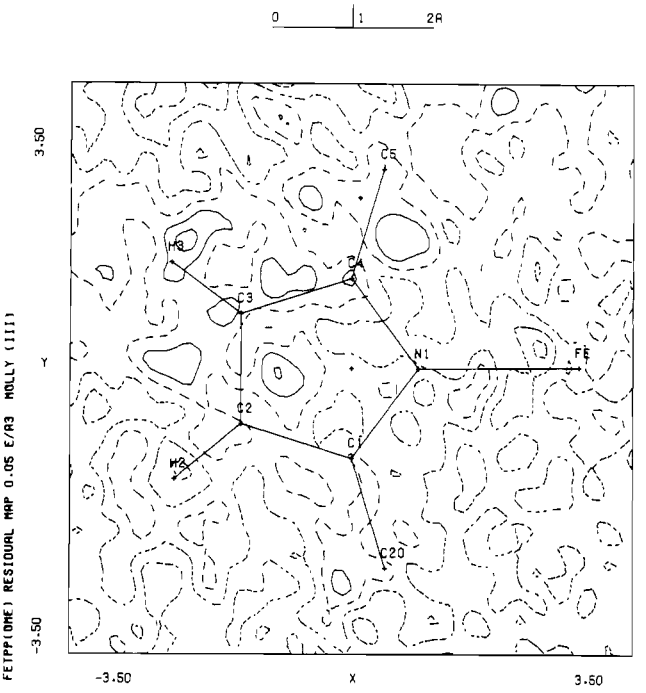

Figure 5. Residual electron density map in the same plane as in Figure 4. Contours are plotted as in Figure 4.

It is interesting to note that the quadrupole splitting of Fe(TPP)Cl, $|\Delta E_{QS}| = 0.48 \pm 0.03$ mm/s, is significantly lower than that of other high-spin ferric porphyrin chlorides.[33] No satisfactory explanation of this anomalous behavior has been presented. Fe(TPP)Cl has been shown to crystallize in the space group $I4/m$ with the molecule disordered about a mirror plane containing the porphyrin ring.[15] Even in an ordered domain of the crystal, charges from neighboring molecules will be aligned along the axial direction. If the distribution of atomic charges is similar to that of $Fe(TPP)OCH_3$, an increased axial contribution would tend to cancel the in-plane contribution, resulting in a net electric field gradient due primarily to q_{val}.

Deformation Density Maps. The multipole model deformation density corresponding to refinement III is plotted in the plane of one of the pyrrole rings in Figure 4. The corresponding map in CoTPP is given in Figure 8 of ref 1. The estimated error distribution in this plane in $Fe(TPP)OCH_3$ is essentially identical with the one calculated for CoTPP and plotted in Figure 3 of ref 1. The high quality of the multipole fit in this plane is evident in the residual map, Figure 5, which shows only random noise with an average deviation from zero of 0.06 $e/Å^3$.

Qualitatively, the deformation maps of $Fe(TPP)OCH_3$ and CoTPP in the pyrrole plane are very similar, as expected from the similarity in their refined multipole populations. One interesting difference, however, is in the size of the C(2)–C(3) bond peak. In $Fe(TPP)OCH_3$, this peak is lower despite the fact that the average bond distance, 1.352 (1) Å, is slightly shorter than the corresponding distance in CoTPP, 1.362 (2) Å. In a comparison of deformation maps of CoTPP and $Fe(TPP)OCH_3$, however, it should be noted that the dynamic maps of the latter could not be calculated to the same high resolution because of computer limitations.

The dynamic deformation density and residual density in a plane containing the iron atom and methoxide ligand are shown in Figures 6 and 7. The quality of the fit is again evident in the low noise and lack of significant features in the residual map. An estimate of the distribution of the standard deviation in this plane is plotted in Figure 8. It is interesting

(33) Dolphin, D. H.; Sams, J. R.; Tsin, T. B.; Wong, K. L. *J. Am. Chem. Soc.* **1978**, *100*, 1711.
(34) Sams, J. R.; Tsin, T. B. In "The Porphyrins"; Dolphin, D., Ed.; Academic Press: New York, 1979; Vol. IV, pp 425–479.
(35) Harris, G. *Theor. Chim. Acta* **1968**, *10*, 119.
(36) Zerner, M.; Gouterman, M.; Kobayashi, H. *Theor. Chim. Acta* **1966**, *6*, 363.
(37) Dolphin, D. H.; Sams, J. R.; Tsin, T. B.; Wong, K. L. *J. Am. Chem. Soc.* **1978**, *100*, 1711.

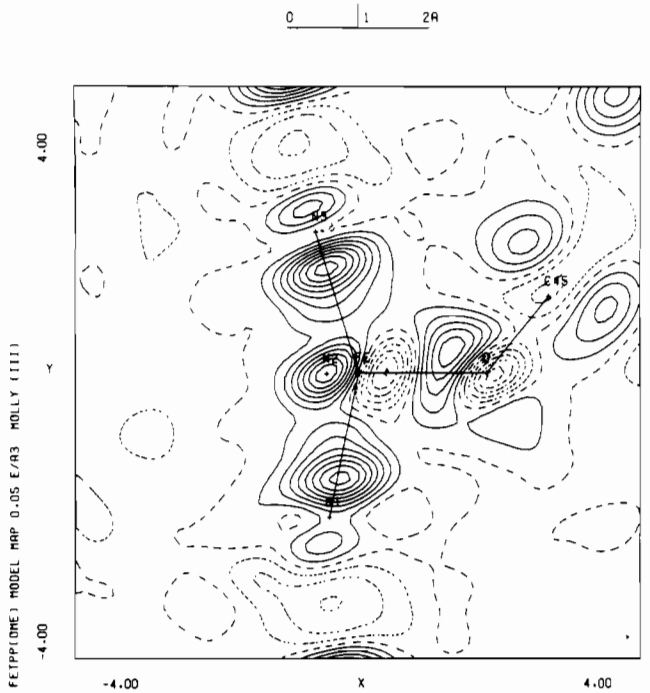

Figure 6. Dynamic model deformation density plotted in a plane passing through the primary iron site and containing the oxygen and carbon atoms of the methoxide ion. Contours are as in Figure 4.

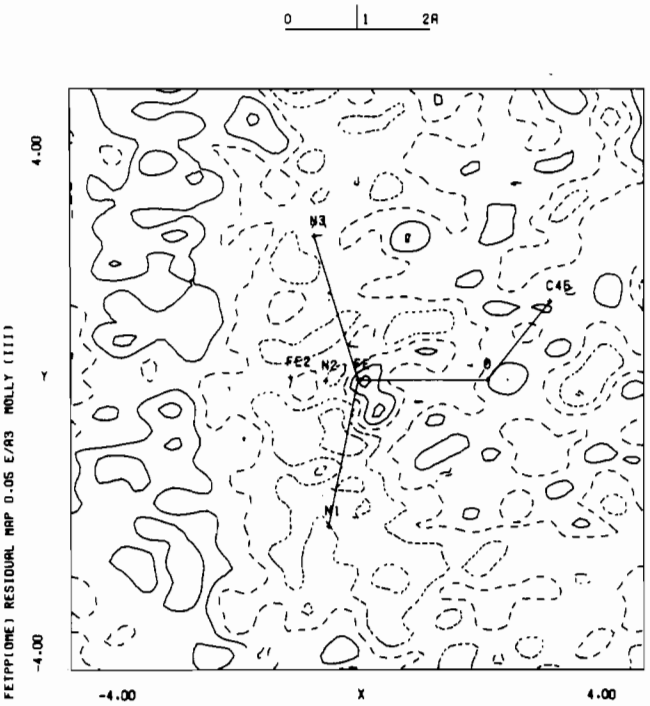

Figure 7. Residual density in the same plane as in Figure 6. Contours are as in Figure 4.

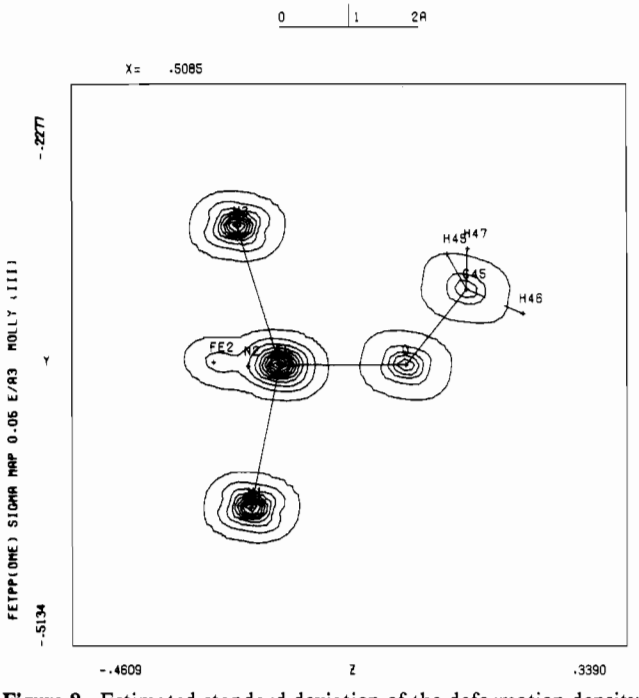

Figure 8. Estimated standard deviation of the deformation density in the plane of Figure 6. Contour intervals are plotted at 0.02 e Å^{-3} intervals with the lowest contour at 0.06 e Å^{-3}.

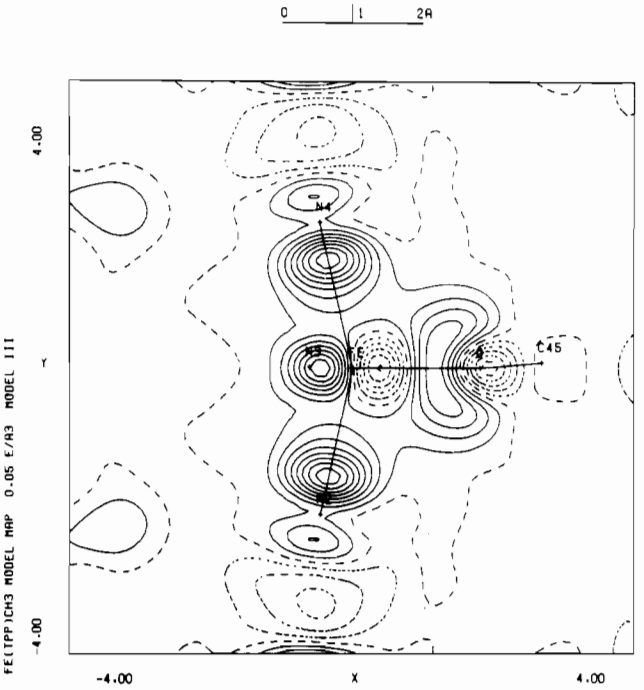

Figure 9. Dynamic model deformation density in a plane that contains the Fe–O bond and is perpendicular to Figure 6. Contours are as defined in Figure 4.

to observe that although the second iron atom has an occupancy of 1.5%, the greater experimental uncertainty associated with its parameters results in a contribution to the estimated standard deviation in the deformation density that is almost as large as that of other atoms.

In Figure 6, peaks are observed in all of the bonds, including the Fe–O and Fe–N bonds. In the Fe–N bonds, the nitrogen "lone pairs" are clearly bent out of the pyrrole plane toward the iron atom, which lies above the plane of the porphyrin ring. A small second lone-pair peak is also evident on the oxygen atom. Oxygen lone-pair features are often found to be sharp and therefore contribute to high-order structure factors. The small size of this peak thus probably reflects the lack of extensive high-order data in the data set and limited resolution in the calculation of the map. A peak near the iron atom on the opposite side from the methoxide ligand is also observed. Since this peak arises primarily from the large P_{10} dipole population on the iron atom, it could only be associated with the d-electron distribution if this distribution is strongly polarized. More likely it reflects remaining deficiencies in the model for the disordered iron site.

A plot of the deformation density in a plane that contains the Fe–O bond and is perpendicular to the plane containing the methoxide ligand (Figure 6) is given in Figure 9. An interesting feature evident in this plane is the quadrupole

deformation on oxygen resulting in a positive density on either side of the Fe–O bond. The hybridization of oxygen appears from the deformation maps to be closer to sp^2 than sp^3, suggesting a π-interaction between Fe and O.

Conclusions

The experimental electron density distribution of a five-coordinate, high-spin iron(III) porphyrin has been obtained from accurate low-temperature X-ray diffraction data. As expected, only small distortions from spherical symmetry are observed for the Fe d-electron distribution, confirming the high-spin nature of the complex. A small quadrupole deformation on the iron atom is observed, producing an electric field gradient at the iron nucleus with positive sign. A contribution of similar magnitude and sign also results from the observed distribution of atomic charges. The total electric field gradient deduced from the X-ray data is in agreement in both sign and magnitude with Mössbauer quadrupole splitting measurements.

With one complete porphyrin molecule in the asymmetric unit, this represents one of the largest charge density studies attempted, in terms of both data collection and computer refinement of results. Although more time and effort was obviously required than for studies of small molecules, the accuracy of the results compares favorably with those from smaller molecules. Also, in this study fewer problems were encountered with the 4s population on the transition-metal atom than in previous studies, probably because the large unit cell results in more low-angle data, which help to define the diffuse density features. It thus appears that the only limitations to studies on large biologically significant molecules will be the requirements that the crystals be of adequate quality and that sufficient instrument and computing time be available.

Acknowledgment. The authors thank Dr. F. Baert for assistance in solving the structure. Support of this work by the National Institutes of Health (Grant HL-23884) and the National Science Foundation (Grant CHE-7905897) is gratefully acknowledged. C.L. is grateful to NATO for providing him with a postdoctoral fellowship.

Registry No. $Fe(TPP)OCH_3$, 29189-59-1.

Supplementary Material Available: Listings of least-squares planes (Table VII), atomic thermal parameters (Table IX), and observed and calculated structure amplitudes (48 pages). Ordering information is given on any current masthead page.

Contribution from the Fakultät für Chemie, Universität Bielefeld, 48 Bielefeld, Federal Republic of Germany

Electronic Structure of Tetraphosphabicyclo[1.1.0]butane

WOLFGANG W. SCHOELLER* and CORNELIA LERCH

Received May 28, 1982

The electronic nature of the title compound tetraphosphabicyclo[1.1.0]butane is analyzed. Accordingly, π'- (π-) donors or acceptors exert considerable effect on the bond lengths of the parent compound. The central bond possesses olefinic character, as is known for the case of bicyclo[1.1.0]butane. The structures of the radical cations are explored. The fragmentation of the title compound as well its reaction to its monocyclic isomer, which is isovalent with N_2S_2, is evaluated.

Although the phospha analogue **1** of bicyclo[1.1.0]butane has been postulated as an intermediate in the reaction of white phosphorus with alkyl halides,[1] its synthesis and structural elucidation have only been verified recently.[2] **1** is isovalent

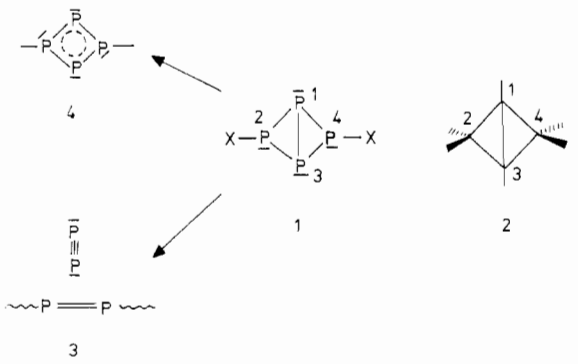

with the well-known bicyclo[1.1.0]butane[3] (**2**). Because of the similarities noted, it is surprising that its structure differs from **2**. In **1** (X = $N(SiR_3)_2$) the bond between the bridgehead atoms P(1)P(3) is shorter by 0.1 Å compared with the bonds to the peripheral phosphorus atoms (P(1)P(3) = 2.128 Å; P(1)P(2) = 2.228 Å.[2] The folding angle between the planes spanned by the three-membered rings is 95.5°. Hence, the central bond P(1)P(3) in **1** is shorter than a PP single bond (2.230 Å in diphosphane[4]) and, at the same time, longer than a PP double bond (2.034 Å in diphenyldiphosphaethylene[5]). In **2** the bridgehead bond C(1)C(3) and the peripheral CC bonds are equal (C(1)C(3) = 1.497 Å; C(1)C(2) = 1.498 Å).[6]

In the present publication we deal with the electronic structure of **1**. In more detail we will evaluate the following aspects in our study: (1) The electronic structure of **1** will be analyzed and compared with that of **2**. (2) A theory of substituent effects on the bonding properties in **1** will be presented. It will be shown that electron-releasing or electron-accepting substituents considerably alter the bonding properties in parent

(1) C. Brown, R. F. Hudson, and G. A. Wartew, *Phosphorus Sulfur*, **5**, 67 (1978); see also H. Quast, *Nachr. Chem., Tech. Lab.*, **27**, 120 (1979).
(2) E. Niecke, R. Rüger, and B. Krebs, *Angew. Chem., Int. Ed. Engl.*, **21**, 544 (1982).
(3) For a discussion of its properties see e.g.: K. B. Wiberg, G. M. Lampman, R. P. Ciula, D. S. Connor, P. Schertler, and J. Lavanish, *Tetrahedron*, **21**, 2749 (1965); K. B. Wiberg and J. Lavanish, *J. Am. Chem. Soc.*, **88**, 5272 (1966); K. B. Wiberg, *Tetrahedron*, **24**, 1083 (1968).
(4) (a) For structural investigations on this compound see: S. G. Frankiss, *Inorg. Chem.*, **7**, 1931 (1968); B. Beagley, A. R. Conrad, J. M. Freeman, J. J. Monaghan, and B. G. Norton, *J. Mol. Struct.*, **11**, 371 (1972); J. R. Durig, L. A. Carreira, and J. D. Odom, *J. Am. Chem. Soc.*, **96**, 2688 (1974); M. Baudler and L. Schmidt, *Z. Anorg. Allg. Chem.*, **289**, 219 (1957); *Naturwissenschaften*, **44**, 488 (1953). (b) For theoretical studies see: R. Ahlrichs, R. Heinzmann, and C. Zirc, *Theor. Chim. Acta*, **43**, 29 (1976); A. H. Cowley, W. D. White, and M. C. Damasco, *J. Am. Chem. Soc.*, **91**, 1922 (1969); J.-B. Robert, H. Marsmann, and J. R. Van Wazer, *J. Chem. Soc. D*, 356 (1970); E. L. Wagner, *Theor. Chim. Acta*, **23**, 127 (1971).
(5) M. Yoshifuji, I. Shima, and N. Inamoto, *J. Am. Chem. Soc.*, **103**, 4587 (1981).
(6) K. W. Cox, M. D. Harmony, G. Nelson, and K. B. Wiberg, *J. Chem. Phys.*, **50**, 1976 (1969).

0020-1669/83/1322-2992$01.50/0 © 1983 American Chemical Society